1-1-1989

Methods for Identifying Footfall Positions for a Legged Robot

C. Caillas
Carnegie Mellon University

Martial Hebert
Carnegie Mellon University, hebert@ri.cmu.edu

E. Krotkov
Carnegie Mellon University

I. S. Kweon
Carnegie Mellon University

Takeo Kanade
Carnegie Mellon University, tk@cs.cmu.edu

Methods for Identifying Footfall Positions for a Legged Robot

C. Caillas, M. Hebert, E. Krotkov, I. S. Kweon, T. Kanade [1]
The Robotics Institute
Carnegie Mellon University
Pittsburgh, Pennsylvania 15213

Abstract

We are designing a complete autonomous legged robot to perform planetary exploration without human supervision. This robot must traverse unknown and geographically diverse areas in order to collect samples of materials. This paper describes how a geometric terrain representation from range imagery can be used to identify footfall positions. First, we present previous research aimed to determine footfall positions. Second, we describe several methods for determining the positions for which the shape of the terrain is nearest to the shape of the foot. Third, we evaluate and compare the efficiency of these methods as functions of some parameters such as particularities of the shape of the terrain. Fourth, we introduce other methods that use thermal imaging in order to differentiate materials.

1 Introduction

We are prototyping a six-legged robot called the Ambler (Figure 1) for an exploratory mission on another planet, possibly Mars [1]. In order to explore new regions and collect samples of materials, the Ambler must traverse unknown and geographically diverse areas.

To accomplish its mission, a critical task for the Ambler is to determine where to place its feet. This task is essential for locomotion over the rugged and irregular terrain that can be encountered on the surfaces of other planets such as Mars, on ocean floors, in hazardous waste sites, and in mines.

The aim of this paper is to present several methods for the Ambler perception system to determine footfall positions. The Ambler perception system consists of a laser range finder and algorithms that build an elevation map of the terrain from range images. The different methods operate on the geometric structure of the terrain, seeking positions for which the shape of the terrain is the nearest to the shape of the foot.

This paper presents in section 2 previous research for the determination of footfalls for legged robots. Section 3 presents several methods for identifying footfall positions based on geometric analysis of the computed elevation map. Section 4 introduces other methods that use information coming from thermal sensors. This paper concludes by discussing the limitations of the previous methods and presenting future work.

[1]This research was sponsored by NASA under Contract NAGW 1175. C. Caillas is on leave of absence from GIAT (FRANCE): Industrial Group for Terrestrial Armements and is supported by DGA (FRANCE): General Delegation for Armement. The views and conclusions contained in this document are those of the authors and should not be interpreted as representing the official policies, either expressed or implied, of NASA or the US Government.

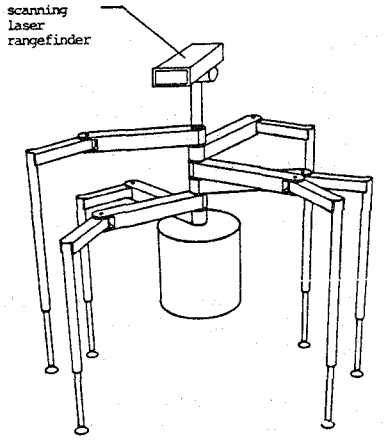

Figure 1: The Ambler

2 Previous research

A legged robot has the possibility to choose where to place its feet. The flexibility in choosing foot placements is one of the mobility advantages of legs over wheels [6]. If a footfall proves inadequate there is the chance of shifting the foot to a new one. To capitalize on this flexibility, two general ways in which walking machines can be controlled to adapt to uneven terrain have been investigated during the last ten years.

The first is for the vehicle to walk forward blindly (without vision) and modify its leg lengths to control orientation. In this case, measurement of *body orientation* and sensing of *force* are essential [9], [12]. Attitude sensing permits the vehicle to control its orientation. Force sensing allows the feet to conform to the terrain since it determines axial and transverse forces on the feet which indicate the attitude of the foot relative to the ground [10]. As complementary to force sensing, *touch sensing* can be used to detect foot ground or object contact [11]. With force or touch sensing, walking speed must be reduced to permit tactile probes of the terrain.

The second approach, that so far has received less attention, is to use proximity and vision sensors. These sensors permit the determination of footfall positions in advance (i.e., before setting the foot on the ground). Proximity sensing indicates the presence of an object within a certain volume, and can be useful for controlling foot placement. With vision sensors, the vehicle can compute an internal model of the geometric structure of the terrain and plan leg trajectories to conform to this model. Furthermore, imaging sensors can give useful information for identifying objects such as

rocks, ditches, or steps. As a first example, Ozguner [4] used a ranging system composed of two cameras and a structured light projector. An operator aboard the robot selects a footfall. This permits utilization of human intelligence in selecting footfalls for arbitrary terrains, but also requires the operator's attention. As a second example, the Adaptive Suspension Vehicle uses the terrain elevation map constructed by a laser scanner for selecting footfalls [5]. Good footfalls correspond to terrain regions where the local computed slope does not exceed a given threshold.

In summary, it appears that little work has been done for determining footfall positions for a legged robot by using imaging sensors. In this paper, we analyze some methods using only imaging sensors, without human supervision.

3 Identifying footfall positions with a laser range finder

In this section, we concentrate on methods using the ERIM laser range finder (described in [2]). The Ambler perception system takes a sequence of range images and constructs an elevation map (the method is described in [2]). Figure 2 schematically illustrates the structure of the elevation map, and Figure 3 depicts an elevation map constructed from four images. The elevation map is then used to find the best foot-shaped subregion $\mathcal{S}$ in a given region $\mathcal{R}$.

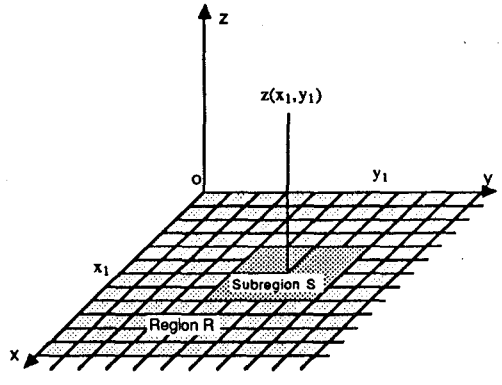

Figure 2: Elevation map representation

We model the foot as a flat disk 30 cm in diameter (Figure 4), and the subregion $\mathcal{S}$ as a square 30 cm in side. The foot plate is orthogonal to the leg. The only possible articulation between the leg and the foot is a rotation around the leg axis that ensures rotation of the leg during walking.

Five methods have been developed, and are presented in increasing order of complexity. All of them are based on the determination of the geometric structure of the terrain.

3.1 Methods

The five methods[2] presented below determine the flattest $\mathcal{S}$ in $\mathcal{R}$. $\mathcal{S}$ is given by the coordinates (x, y) of the center of the foot on the elevation map. More generally, the applied methods determine, for every possible subregion $\mathcal{S}$ in $\mathcal{R}$, a value that characterizes $\mathcal{S}$ in terms of position goodness. The smallest value corresponds to the "best" position, and the largest to the "worst." The other positions receive intermediate values. In the following, we note $N_k(x, y)$ the

[2]The principle of these methods is summarized in [3].

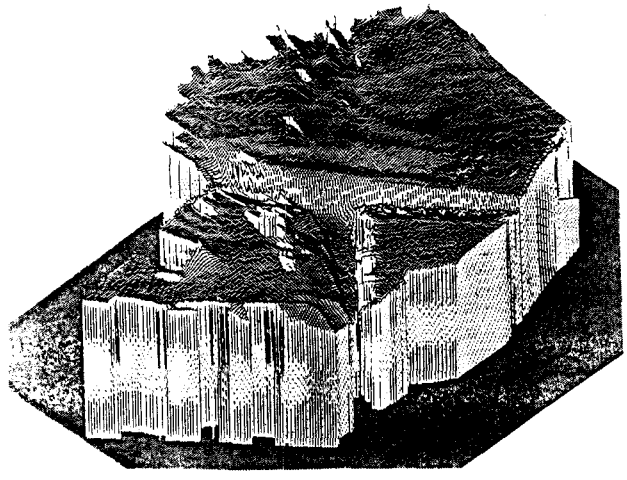

Figure 3: Elevation map of rugged terrain

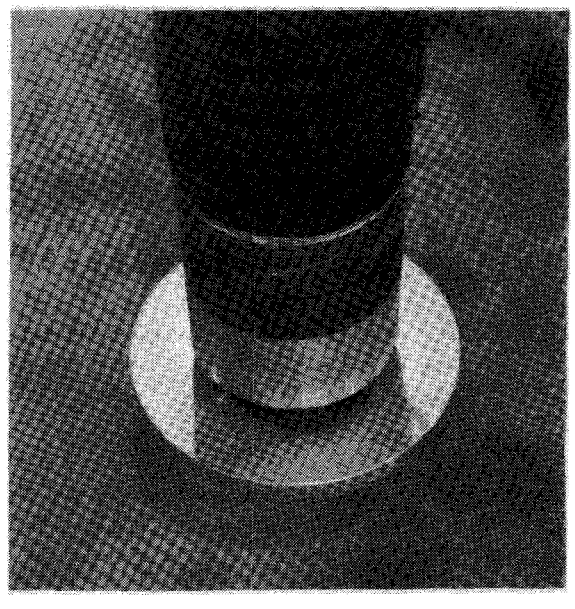

Figure 4: Foot of the Ambler

value attributed by the algorithm numbered k (k = 1 to 5 for the five methods) to the position (x, y). For every position (x, y) of the center of the foot in $\mathcal{R}$, $N_k(x, y)$ depends not only on the position (x, y) but also on the elevations of all the points of the terrain just under the foot (i.e. within $\mathcal{S}$). This may be written

$$N_k(x, y) = f(z(x_1, y_1), ..., z(x_n, y_n)) , \quad (1)$$

such that $\forall i \in \{1, n\}\ |x_i - x| < \frac{d}{2}\ \&\ |y_i - y| < \frac{d}{2}$, and f represents the function of flatness. In the following $z(x_i, y_i)$ will be noted z_i to simplify the notation.

3.1.1 Max-Min

The idea of the method is to find $\mathcal{S}$ in $\mathcal{R}$ that minimizes the difference between the maximum and the minimum elevation (see Figure 5).

The function N_k can be written

$$N_1(x, y) = z_{max} - z_{min} , \quad (2)$$

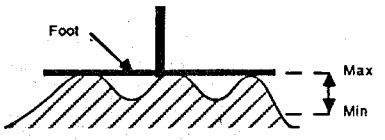

Figure 5: Max-Min applied to the foot shape

where $k = 1$ designates the Max-Min algorithm.

If $N_1(x, y) = 0$, then S is perfectly flat. Generally, this type of surface is not observed in natural environments. However, according to the criteria presented above, the lower is $N_1(x, y)$, the "nearer" the shape of the terrain is to a plane. Thus, all the shapes of the terrain for which $N_1(x, y)$ takes the minimum value are suitable.

Since this method measures the difference between the maximum and the minimum of the elevation, it does not differentiate a single spike and an undulating surface for which this difference is the same (see Figure 6).

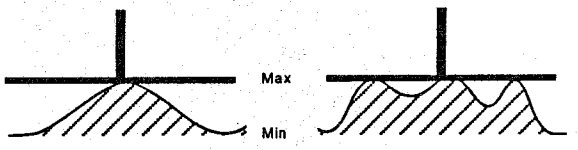

Figure 6: Single spike (left) and undulating surface (right)

To that extent, this method does not take into account the shape of the surface. This is undesirable since the undulating shape is nearer to a plane than the single spike.

3.1.2 Plane Fit

The Plane Fit method determines the position (x, y) that minimizes

$$N_2(x, y) = \frac{1}{n} \sum_{i=1}^{n} (z_i - z_{plane})^2 , \tag{3}$$

where z_i is the elevation of the point i (see Figure 7). z_{plane} is the elevation of the plane that averages the set of points i:

$$z_{plane} = \frac{1}{n} \sum_{i=1}^{n} z_i . \tag{4}$$

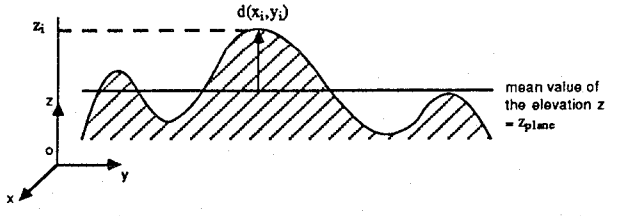

Figure 7: Plane Fit algorithm

Note that $N_2(x, y) = 0$ is equivalent to $\forall\, i \in \{1, n\}\ z_i = z_{plane}$. Hence, $N_2 = 0$ implies that S is planar.

The normal distance $d_i = d(x_i, y_i) = z_i - z_{plane}$ between the point i and the mean plane is called the roughness[3] of the surface at the point i [7]. It is however difficult to give a definite definition of the roughness. This notion has been revisited in [8] where the roughness is presented as a vector that depends on the amplitude but also on the frequency and some autocorrelation components. The subregion S for which $N_2(x, y)$ is minimum, best fits the plane thus found.

3.1.3 Support Area

This method takes into account the constraint of minimizing the amount of energy necessary to achieve the minimum support area. The energy depends on two parameters: the depth of penetration into the soil; and the force exerted by the foot on the soil during penetration. The foot ceases to penetrate when the force on the soil equals the force exerted by the soil. The depth and the force of penetration (or more accurately the pressure) depends on the type of soil. There are many types of soil such as sand or damp ground for which the following formula, that relates the depth of penetration δ and the pressure P exerted by the foot, can be applied:

$$P = k\delta^n , \tag{5}$$

where k and n are constants that depend on the type of soil, and can be determined by experiment. This formula is the simplest formula which agrees with experimental results [12], and allows to calculate the energy E spent during the penetration of the foot. If the contact surface $S(\delta)$ required to stop the penetration of the foot is reached for $\delta = \delta_{opt}$ then

$$E = \int_0^{\delta_{opt}} P(\delta)\, S(\delta)\, d\delta , \tag{6}$$

where $S(\delta)$ is a function of the distance δ traveled along the vertical direction (see Figure 8).

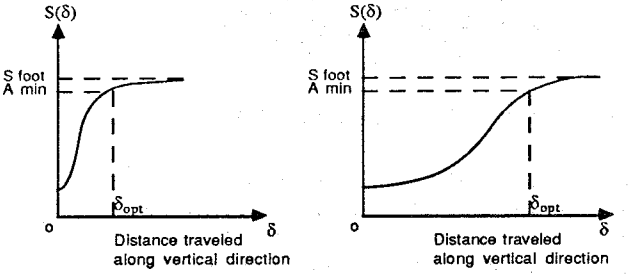

Figure 8: Support area as function of the distance traveled along the vertical direction

If the type of soil is known, the parameters k and n are known. The above formula shows that the energy is minimum when the integral is minimum. Since $P(\delta)$ and $S(\delta)$ increase with δ, the product of these two functions increases with δ. Therefore, $E < P(\delta_{opt})S(\delta_{opt})\delta_{opt}$. Thus, the integral is minimum when δ_{opt} is minimum. However, this result is not rigorously correct. The function $S(\delta)$ can reach δ_{opt} very smoothly or very quickly with δ (see the two cases in Figure 8). Of course, E is minimized in the

[3]The roughness is described by a function $d(x, y)$ that gives the height of the surface above or below the average surface at any position (x, y) of the surface.

smooth case. Our algorithm does not take this into account; we assume that in first approximation it can be neglected.

The Support Area algorithm has the same meaning as the Max-Min algorithm when the minimum support area is taken equal to the surface of the foot. In both cases, the algorithm aims to minimize the difference between the maximum and the minimum of the elevation or the depth of penetration to reach the minimum support area.

3.1.4 Free Volume

The Free Volume algorithm calculates the unoccupied volume located between the foot plate and the surface of the terrain (see Figure 9). The best subregion S minimizes the free volume.

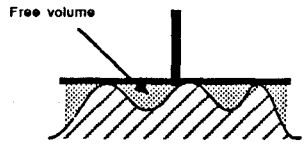

Figure 9: Free volume under the foot

Let V be the free volume:

$$V = \int_{x-d/2}^{x+d/2} \int_{y-d/2}^{y+d/2} (z_{max} - z(u,v))dudv \ , \qquad (7)$$

where (x, y) is the center of the foot. An approximation of this expression can be calculated with the elevation map data. If n is the number of elevation map samples just under the foot, then

$$V(n) = \frac{d^2}{n^2} \sum_{i=1}^{n} (z_{max} - z_i) \ , \qquad (8)$$

where $V = \lim_{n\to\infty} V(n)$. The number of samples n has to be big enough to limit the error $\epsilon(n)$, where $\epsilon(n) = V - V(n)$.

This method correctly discriminates surfaces that the Max-Min algorithm can not distinguish. For instance, the Free Volume algorithm differentiates the single spike and the undulating surface presented in Figure 5.

Minimizing $N_1(x, y) = z_{max} - z_{min}$ implies minimizing $N_1(x, y)d$, which represents the volume located just under the foot, between the two planes located at the elevations z_{min} and z_{max}. This volume is always inferior to the unoccupied volume located between the foot and the ground. Furthermore, there are an infinity of surface shapes for which $(z_{max} - z_{min})d$ is the same but the unoccupied volume different. The Free Volume is therefore more precise than the Max-Min algorithm for the determination of flat surfaces.

3.1.5 Equilibrium

This algorithm is complementary to the Free Volume algorithm in the sense that it finds S that minimizes the free volume V and the first moment M. The first moment of the mass distribution about the foot is

$$M = \sqrt{m_x^2 + m_y^2}$$

$$m_x = \sum_{i=1}^{n} y_i(z_{max} - z_i)$$

$$m_y = \sum_{i=1}^{n} x_i(z_{max} - z_i)$$

This algorithm is in two steps. First, the algorithm selects the subregions S for which the free volume is under $(1 + x)V_{min}$. (x was chosen between 5 and 10 percent). Second, the algorithm chooses, among the subregions S found at the first step, that one for which M takes the lowest value.

S found by this algorithm is relatively flat since the free volume is near to the minimum free volume. The minimization of M allows the foot to be in equilibrium on the terrain. On the other hand, when the foot contacts sandy soil, the sand fills the holes with the minimum of penetration to reach the maximum contact area between the foot and the soil.

3.2 Comparison and evaluation of the different methods

3.2.1 Theoretical approach

In order to evaluate the different methods we analyze in this section their behavior on several terrain shapes such as step, slope, and undulating surface. For simplicity, the analysis assumes that the terrain surface is given by a two-dimensional continuous function (i.e., not a discrete elevation map).

Step

An ideal step can be defined by two parameters, its height h and its length l.

1) The Max-Min algorithm calculates the height h of the step: $N_1(x, y) = h$. It does not take into account the width of the step, and thus does not differentiate a wide step from a small one.

2) The Plane Fit algorithm calculates $N_2(x, y) = \frac{h^2}{d^2} l(d - l)$ if $d \geq l$, and 0 if $d < l$ (the mean value of the step function is $z_{plane} \approx h\frac{l}{d}$). This is a general expression independent of n, that vanishes with h, l and $d - l$. $h = 0$ and $d \leq l$ both correspond to a plane for the support area. $l = 0$ corresponds to a plane only if $h = 0$ and a single spike otherwise. Therefore, the Plane Fit algorithm does not differentiate a flat region from a single spike.

3) The Support Area algorithm calculates the depth of penetration in the step. If l exceeds the minimum support area required to support the foot, then the depth of penetration is zero. In this case, the method does not distinguish a high step from a small step. This is undesirable. If l is lower than the minimum support area, then the depth of penetration is h. In this case, the Support Area algorithm has the same meaning as the Max-Min algorithm.

4) The Free Volume method calculates the free volume V located under the foot. For the step, $V = (d - l)h$. Therefore, V decreases as h decreases, and as l approaches d (i.e., as the surface approaches a plane). Thus, the Free Volume algorithm discriminates correctly the flat regions from the others, since the step corresponds locally (i.e. under the foot) to a perfect plane. However, this method does not distinguish the two cases presented in Figure 10, since $N_3(x, y) = V$ is the same.

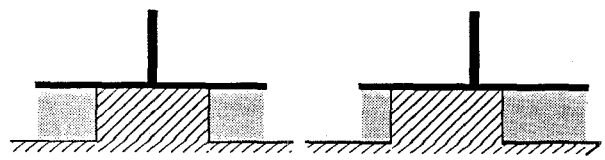

Figure 10: Equilibrium: influence of the position of the foot on the step

5) The Equilibrium method calculates the moment M about the z-axis of the "holes" situated under the foot. Let p be the distance between the center of the step and the center of the foot. For the step, $M = ph$. Therefore, M vanishes with p and h. This method allows us to differentiate the two cases presented in Figure 11 by selecting the symmetric case that corresponds to $M = 0$.

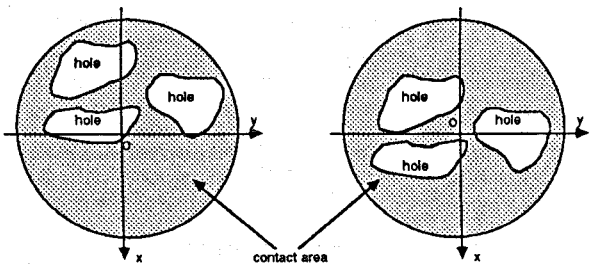

Figure 11: Mass distribution about the z axis of the foot

Slope

A slope can be defined by one parameter: the slope angle θ.

1) The Max-Min algorithm calculates the following expression: $N_1(x, y) = z_{max} - z_{min} = d \tan\theta$.

2) The Plane Fit method calculates the following expression: $N_2(x, y) = \frac{d^3}{12} \tan^2\theta$.

3) The Support Area method calculates $N_3(x, y) = \frac{d}{2} \tan\theta$ for a minimum support area taken equal to $\frac{d}{2}$.

4) The Free Volume method calculates the unoccupied volume located between the foot and the slope: $N_4(x, y) = \frac{d^2}{2} \tan\theta$.

5) The Equilibrium algorithm calculates $N_4(x, y)$ and $N_5(x, y)$. The calculation of $N_5(x, y)$ is not necessary since $N_5(x, y) = \frac{1}{2} N_4(x, y)$.

For the slope, $N_1, ..., N_5$ are minimized with θ. The five algorithms discriminate correctly flat regions.

Undulating Surfaces

As undulating surfaces, we use sinusoids that are characterized by two parameters: their frequency f; and their amplitude a.

1) The Max-min algorithm calculates the amplitude a of the sinusoid and does not take into account its frequency f. The result is $N_1(x, y) = a$. This algorithm does not distinguish a high frequency sinusoid from a low one.

2) The Plane Fit algorithm calculates $N_2(x, y) = \frac{a^2}{2}(1 - \frac{\sin(4\pi fd)}{4\pi fd})$. Thus, the result depends both on a and f, vanishes with a, and approaches $\frac{a^2}{2}$ when f approaches the high frequencies. This method cannot distinguish sinusoids whose frequencies are multiples of $\frac{1}{2d}$.

3) The Support Area algorithm calculates the depth of penetration into the sinusoidal surface to reach the minimum support area. We assume that the minimum support area is one half of the surface of the foot. If the frequency of the sinusoidal surface is large enough ($df > 1$), then the depth of penetration is equal to a, and is independent of f.

4) The Free Volume algorithm calculates $N_3(x, y) = ad(1 - \frac{1}{2\pi fd}(1 - \cos 2\pi fd))$. Like the Plane Fit, this method cannot distinguish sinusoids whose frequencies are mutiples of $\frac{1}{d}$, since $N_3(x, y) = ad$, which is independent of f.

5) The Equilibrium algorithm calculates $N_4(x, y) = 0$ if the sinusoid is symmetric about the z-axis.

Scanner resolution and accuracy

The accuracy of the elevation map significantly affects the results of the algorithms. Simply stated, the number of points sampled in a region equal to the size of the foot can not be too small, and the uncertainty of the computed elevations can not be too large.

The elevation map accuracy depends on two main parameters: the distance D from the scanner to the object (terrain); and the angle θ between the incident laser beam and the object. If the dimensions of the foot ($0.3m$) are much smaller than the object distance D ($\sim 10m$), then in a first approximation, the accuracy is the same for all the measured points located under the foot. Hence, the elevations of all points in S are known with the same error, which is on the order of 5 to $10cm$ for a distance of observation of 5 to $20m$ [2]. Thus, the elevation error may be on the order of 25 percent of the foot diameter. This error is of great significance, and limits the effectiveness of the methods developed.

In the near future, we will use a laser range finder with finer resolution ($\sim 1cm$ instead of $\sim 5cm$) and higher accuracy.

3.2.2 Experimental approach

To evaluate the different methods, we performed some experiments in a realistic environment: a single leg testbed composed of one leg, a $30m^2$ sand box, and a laser range finder mounted above the leg (see Figure 12).

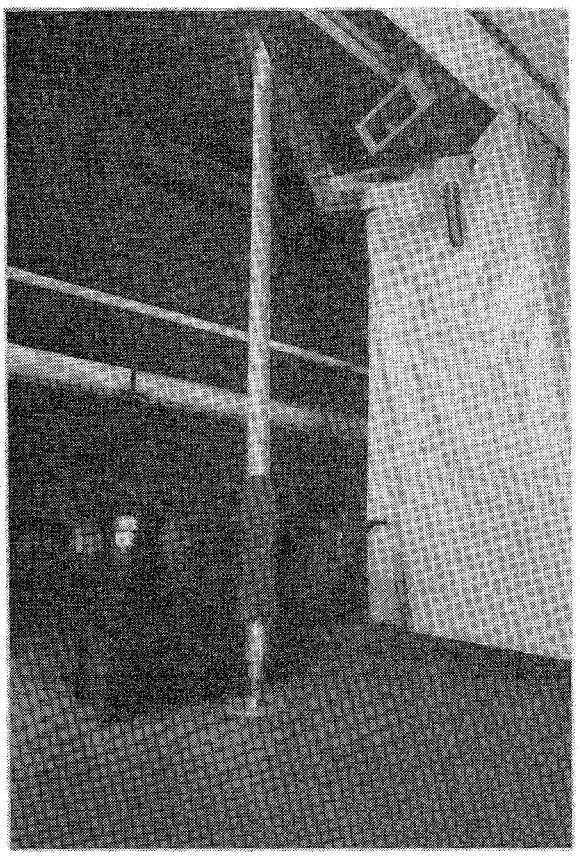

Figure 12: Single leg testbed

Because of the difficulty in defining an absolute ground truth, the experiments do not seek to determine whether one algorithm

is "better" than another one, with respect to ground truth. Instead, they aim to answer the following question: To what extent do the different algorithms agree with each other?

The experimental procedure is as follows.

1) Acquire range images of the terrain, and build an elevation map at 10 cm resolution.

2) Divide the elevation map into $R = 16$ regions $\mathcal{R}$, each of area $1m^2$. These dimensions correspond to the size of the region that planning modules consider in walk planning. The different regions contain various shapes of terrain, ranging from flat to very rough.

3) For each region $r = 1, ..., 16$, for each algorithm $k = 1, ..., K$, compute the "best" footfall position $(x_{k,r}, y_{k,r})$. We expect the computed positions to differ, so in general, for each region there are $K = 5$ different footfall positions.

4) For each region $r = 1, ..., R$, for each computed footfall position $(x_{k,r}, y_{k,r})$ $k = 1, ..., K$, for each algorithm $l = 1, ..., K$ with $l \neq k$, evaluate the algorithm on the footfall position computed by each of the other algorithms $N_l(x_{k,r}, y_{k,r})$. This yields R tables, each with $K \times K - 1 = 20$ values.

5) Normalize the data by

$$n_k(x_{l,r}, y_{l,r}) = \frac{N_k(x_{l,r}, y_{l,r}) - N_k(x_{k,r}, y_{k,r})}{\max(N_{k,r}) - N_k(x_{k,r}, y_{k,r})} , \qquad (9)$$

where $N_k(x_{k,r}, y_{k,r})$ is by definition the minimum value, and $max(N_{k,r})$ is the maximum value determined by the k^{th} algorithm applied to the r^{th} region. Therefore, $0 \leq n_k(x_{k,r}, y_{k,r}) \leq 100$ percent. The smaller is $n_k(x_{k,r}, y_{k,r})$, the greater is the agreement between methods l and k.

6) Calculate the mean values $< n_k(x_l, y_l) >$ over all R regions by

$$< n_k(x_l, y_l) >= \frac{1}{R} \sum_{r=1}^{R} n_k(x_{l,r}, y_{l,r}) . \qquad (10)$$

The resulting table, filled with the mean values, describes the mean behavior of the different methods.

	Max-Min	Plane Fit	Sup Area	Free Vol
Max-Min	0	4	9	6.5
Plane Fit	8	0	22	15.5
Sup Area	34.5	43.5	0	28.5
Free Vol	8.5	10.5	6	0
Equilibrium	2	3	12.5	5.5

7) Calculate the mean value $< n_k >$ for each row of this table by

$$< n_k >= \frac{1}{K-1} \sum_{l=1}^{K-1} n_k(x_l, y_l) . \qquad (11)$$

The values of the k^{th} row of the table represent the goodness given by the different algorithms for the best positions found by the k^{th} algorithm. Therefore, $< n_k >$ represents a global measure of the agreement of all the methods relating to the methods k.

All of the algorithms seem to agree very well with the Max-Min, Free Volume and Equilibrium algorithms since the error is about 5 percent. The error between the Plane Fit and the other algorithms is on the order of 12 percent, while this error is more than 25 percent for the Support Area algorithm. Figure 13 summarizes these results, which indicate that the Support Area and the Plane Fit methods produce results that differ significantly from the three others.

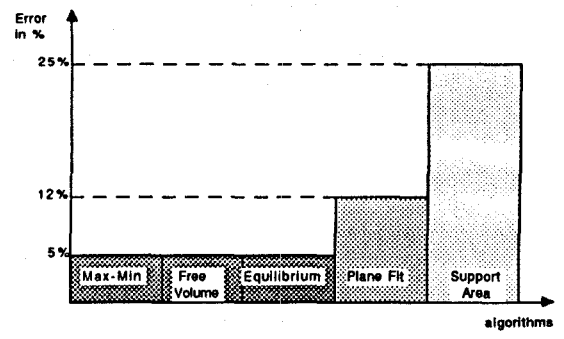

Figure 13: Agreement between the different methods

4 Non-geometric criteria

Understanding the geometry of the terrain is necessary to determine good positions for the feet of the Ambler. Although necessary, this is not sufficient to identify safe footfall positions. For example, there are many cases of flat terrain that is too soft, slippery, or unstable to provide support. Information about soil properties is therefore needed in order to predict when one of the feet might sink into sand or soil, or when the soil is slippery or dangerous.

We can not extract this information from the laser range finder. We could infer it from devices such as force sensors or accelerometers [6]. Probes of the terrain can measure ground hardness, temperature, moisture, and can provide information on the likelihood of sinking and slipping. Alternatively, we could acquire information about soil properties from passive imaging sensors such as black and white and color cameras. The problem of extracting information from visible light sensors is fairly well studied, and much can be done with them.

However, we seek to study a relatively new source of information: thermal imagery. This has not received great attention in robotics, and few studies can be found about it in the literature. In this section, we sketch how a thermal camera can be used to constrain the footfall selection problem.

A thermal camera delivers an image of the scene in which the pixel intensity is a function of the temperature. Generally, warmer points appear brighter, and cooler points appear darker.

The temperature T of the surface of a body is determined by considering its heat exchanges with the environment. The exchange of heat is characterized by four components: the incident solar radiation that is the source of heat; the radiative energy lost by radiation; the conductive and the convective energy that are the heat lost by conduction with the environment and the heat transmitted by convection into the interior of the body. An analytic expression of the surface temperature of an object can be calculated by making several assumptions on the heat exchanges [13]. In particular, the assumption of a semi-infinite body, requiring that the dimensions of the object be sufficiently large. The temperature T is

$$T = T(x, y, z) = f(I, t, p, q) , \qquad (12)$$

where $T(x, y, z)$ is the temperature at the point (x, y, z), I is the thermal inertia, t is time, and (p, q) is the the orientation of the patch of surface at (x, y, z) given by its gradient.

The thermal inertia I is characteristic of the material, and is related to its density, its specific heat, and its thermal conductivity

by the relation $I = \sqrt{k\rho c}$[4]. It is possible to derive I as a function of T, t, p and q by inverting the previous equation: $I = g(T, t, p, q)$ [13]. The knowledge of I at every points–or more precisely, for every patch of surface of the region $\mathcal{R}$—should allow in some degree to determine the nature of the material. For example, sand and rock are the two main constituents of the planet Mars, and should be distinguishable by determining their thermal inertia.

We anticipate undertaking experimental work with such sensors, in order to verify this analysis. Specifically, we intend to identify the orientation of the different surface patches from the elevation map constructed from range data (see Section 3).

5 Discussion

In this paper, we presented several methods to determine good footfall positions for a legged robot.

Unlike other sensors, imaging sensors allow, in some degree, to determine in advance the goodness of footfall positions. This possibility is a great advantage relative to other sensors that require moving to the selected footfall to determine if the footfall is good or not. Since energy minimization is crucial for a complete autonomous robot, preselection decreases the energy and time required for walking.

The geometric methods presented in section 3.1 show that it is possible to use elevation maps to select flat footfall positions. Among the five methods that we developed, the Max-Min, Free Volume, and Equilibrium methods exhibit similar theoretical behavior. The experiments show that these three methods agree very well with the "common sense" of flat regions. The Plane Fit and Support Area methods do not agree so well with the other methods and do not always give experimental results compatible with common sense of footfall positions. The theoretical analysis of section 3.2.1 in part explains the divergence of these two methods.

We will use the Free Volume method as part of the Ambler perception system. Its theoretical performance on terrain consisting of steps, slopes, and undulating surfaces is superior, and its empirical performance is satisfactory. Further experimental work is needed to better characterize this method, and to take into account the geometric uncertainty due to the laser scanner resolution.

Geometric methods are insufficient to ensure that a footfall position is completely safe. The approach of Section 4 for using other imaging sensors seems promising to discriminate different kinds of material such as rock or sand. We intend to experiment with thermal cameras to evaluate whether their practical performance lives up to their theoretical promise. We expect that fusion of information from different imaging sensors will allow identification of safe footfall positions.

For the future, we must also integrate other sensors that measure directly and precisely other features of the soil, such as compliance, load-bearing strength, and coefficient of friction.

References

[1] J. Bares, M. Hebert, T. Kanade, E. Krotkov, T. Mitchell, R. Simmons, and W. Whittaker. An Autonomous Rover for Planetary Exploration. *IEEE Computer*, vol. 22, pp. 18-26, June 1989.

[2] M. Hebert, T. Kanade, and I. Kweon. *3-D Vision Techniques for Autonomous Vehicles*. Technical Report CMU-RI-TR-88-12, The Robotics Institute, Carnegie Mellon University, 1988.

[3] M. Hebert, C. Caillas, E. Krotkov, I. S. Kweon, T. Kanade. Terrain Mapping for a Roving Planetary Explorer. *IEEE Robotics and Automation Conference*, Scottsdale, Arizona, May 1989.

[4] F. Ozguner, S. J. Tsai, and R. B. McGhee. An Approach to the Use of Terrain-Preview Information in Rough-Terrain Locomotion by a Hexapod Walking Machine. *International Journal of Robotics Research*, 3(2): 134-146, Summer 1984.

[5] T. E. Bihari, T. M. Walliser, and M. R. Patterson. Controlling the Adaptive Suspension Vehicle. *IEEE Computer*, vol. 22, pp 59-65, June 1989.

[6] D. J. Todd. Walking Machines. *An Introduction To Legged Robots*. Chapman and Hall. 1985.

[7] H. E. Bennett, J. O. Porteus. Relation Between Surface Roughness and Specular Reflectance at Normal Incidence. *Journal of the Optical Society of America*, vol. 51, pp. 123-129. 1961.

[8] R. Hoffman and E. Krotkov. Terrain Roughness Measurement from Elevation Maps. In *Proceedings of SPIE Advances in Intelligent Robotics Systems*, Philadelphia, Pennsylvania, To appear, November 1989.

[9] C. A. Klein, K. W. Olson, D. R. Pugh. Use of Force and Attitude Sensors for Locomotion of a Legged Vehicle over Irregular Terrain. *International Journal of Robotics Research*, 2(2): 3-17, Summer 1983.

[10] K. J. Waldron. Force and Motion Management in Legged Locomotion. *IEEE Journal of Robotics and Automation* 2(4): 214-220 December 1986.

[11] P. K. Allen. Intergration Vision and Touch for Object Recognition Tasks. *International Journal of Robotics Research*, 7(6): 15-33, December 1988.

[12] M. Kaneko, K. Tanie, M. Than. A Control Algorithm for Hexapod Walking Machine Over Soft Ground. *IEEE Journal of Robotics and Automation*, 4(3): 294-302, June 1988.

[13] C.Caillas. *Infrared Thermal Camera for Autonomous Vehicles*. Technical Report, The Robotics Institute, Carnegie Mellon University, To appear, fall 1989.

[4] The thermal inertia for thin dry sand is about $270 Ws^{\frac{1}{2}}/m^2K$, and it is about $2200 Ws^{\frac{1}{2}}/m^2K$ for rocks.